

Effect of non-stoichiometry on the structure and microwave dielectric properties of $\text{BaMg}_2\text{V}_2\text{O}_8$ ceramics

WeiQiong Liu¹ · Yang Wang¹ · Ruzhong Zuo¹

Received: 10 June 2017 / Accepted: 11 July 2017 / Published online: 14 July 2017
© Springer Science+Business Media, LLC 2017

Abstract The effect of the A-site non-stoichiometry on the crystal structure, microstructure and microwave dielectric properties of $\text{Ba}_{1+x}\text{Mg}_2\text{V}_2\text{O}_8$ ceramics was investigated in this work. The X-ray diffraction results show that the $\text{BaMg}_2\text{V}_2\text{O}_8$ solid solution was formed in the composition range of $-0.02 \leq x \leq 0.02$ while a secondary phase $\text{Ba}_3\text{V}_2\text{O}_8$ started to appear at $x \geq 0.04$, as confirmed by scanning electron microscopy and energy dispersion spectrum. The introduction of a slightly excessive Ba^{2+} into the matrix lattice could enhance the quality factor ($Q \times f$) owing to the improved sinterability while overmuch Ba^{2+} would deteriorate $Q \times f$ due to the presence of the high-loss $\text{Ba}_3\text{V}_2\text{O}_8$ phase. The maximum $Q \times f$ value of 192,840 GHz was obtained at $x = 0.01$. The temperature coefficient of the resonant frequency (τ_f) changed little as $-0.02 \leq x \leq 0.02$ and then monotonically increased up to a positive value as $0.02 < x \leq 0.52$. Near-zero τ_f value was obtained at $x = 0.44$ owing to the formation of the composite between the secondary-phase $\text{Ba}_3\text{V}_2\text{O}_8$ and the matrix-phase $\text{BaMg}_2\text{V}_2\text{O}_8$. In general, excellent microwave dielectric properties of $\epsilon_r = 12.4$, $Q \times f = 192,840$ GHz, $\tau_f = -35.9$ ppm/°C and $\epsilon_r = 13.7$, $Q \times f = 92,580$ GHz, $\tau_f = -5.3$ ppm/°C were achieved in $\text{Ba}_{1.01}\text{Mg}_2\text{V}_2\text{O}_8$ ceramics sintered at 915 °C for 4 h and $\text{Ba}_{1.44}\text{Mg}_2\text{V}_2\text{O}_8$ ceramics sintered at 930 °C for 4 h, respectively.

1 Introduction

With the rapid development of the microwave communication technology, microwave dielectric ceramics with high performances are in great demands [1]. Particularly, the low-temperature cofired ceramic (LTCC) technology has played an increasingly important role in the fabrication of modern electronic devices, which would require dielectric ceramics to have a low sintering temperature below the melting point of silver (961 °C) in addition to desirable microwave dielectric properties [2].

Recently, some Bi_2O_3 -, MoO_3 -, B_2O_3 -, Li_2O -, and V_2O_5 -based microwave dielectric ceramics have gained considerable attention due to their intrinsically low sintering temperatures [3–9]. Among them, many vanadate ceramics have both a low sintering temperatures and good microwave dielectric properties, which make them become potential candidates in LTCC technology. $\text{BaMg}_2\text{V}_2\text{O}_8$ with a body-centered tetragonal structure was reported to possess excellent microwave dielectric properties of $\epsilon_r = 12$, $Q \times f = 156,140$ GHz (9.9 GHz) and $\tau_f = -36$ ppm/°C at a relatively low sintering temperature of 900 °C [10]. However, the undesirable τ_f value of -36 ppm/°C precluded its immediate application in LTCC.

The common method to tailor τ_f value is to add some materials with opposite-sign τ_f , such as $\text{Ba}_3(\text{VO}_4)_2\text{-Mg}_2\text{SiO}_4$ and $\text{Ca}_5\text{Mg}_4(\text{VO}_4)_6\text{-Ba}_3(\text{VO}_4)_2$ system [11, 12]. Wang et al. reported that adding 13% TiO_2 in $\text{BaMg}_2\text{V}_2\text{O}_8$ has successfully tailored the negative τ_f value, and good microwave dielectric properties of $\epsilon_r = 13.0$, $Q \times f = 97,334$ GHz and $\tau_f = -4$ ppm/°C were obtained at 900 °C for 4 h [10]. Moreover, the ionic substitution was also widely used in tailoring undesirable τ_f values, such as $(\text{Zn}_{1-x}\text{Ni}_x)_3\text{Nb}_2\text{O}_8$ and $\text{Co}(\text{Ti}_{1-x}\text{Zr}_x)\text{Nb}_2\text{O}_8$ system [13, 14]. Similarly, the Sr^{2+} substitution

✉ Ruzhong Zuo
rzzuo@hotmail.com

¹ Institute of Electro Ceramics & Devices, School of Materials Science and Engineering, Hefei University of Technology, Hefei 230009, People's Republic of China

for Ba^{2+} in $\text{Ba}_{1-x}\text{Sr}_x\text{Mg}_2\text{V}_2\text{O}_8$ system also made the τ_f value experience a considerable variation from negative to positive values as a result of increasing the A-site bond valence. Desirable microwave dielectric properties of $\epsilon_r=13.3$, $Q \times f=86,640$ GHz and $\tau_f=-6$ ppm/ $^\circ\text{C}$ were achieved in $\text{Ba}_{0.85}\text{Sr}_{0.15}\text{Mg}_2\text{V}_2\text{O}_8$ ceramics sintered at 915°C for 4 h [15]. In addition, non-stoichiometry also plays an important role in improving dielectric performances of the matrix ceramics. It was reported that the $Q \times f$ value of $\text{Ba}[(\text{Co}_{0.7}\text{Zn}_{0.3})_{1/3}\text{Nb}_{2/3}]\text{O}_3$ was greatly enhanced by A-site non-stoichiometry for the increased long-range order degree, although the τ_f value was tailored at the same time. Microwave dielectric properties of $\epsilon_r=33.7$, $Q \times f=70,917$ GHz and $\tau_f=-4.07$ ppm/ $^\circ\text{C}$ were achieved in $\text{Ba}_{0.99}[(\text{Co}_{0.7}\text{Zn}_{0.3})_{1/3}\text{Nb}_{2/3}]\text{O}_3$ [16]. Similar phenomenon also occurred in $\text{Ba}_{1+x}(\text{Mg}_{1/3}\text{Ta}_{2/3})\text{O}_3$ system, where the optimal microwave dielectric properties of $\epsilon_r=24.7$, $Q \times f=152,580$ GHz and $\tau_f=1.2$ ppm/ $^\circ\text{C}$ were achieved [17]. Therefore, A-site non-stoichiometry was also expected to bring out a great improvement in microwave dielectric properties of $\text{BaMg}_2\text{V}_2\text{O}_8$ ceramics. In this work, the $\text{Ba}_{1+x}\text{Mg}_2\text{V}_2\text{O}_8$ ($x=-0.02$ to $+0.52$) ceramics were prepared and their phase composition, microstructure and microwave dielectric properties were investigated systematically.

2 Experimental procedure

The $\text{Ba}_{1+x}\text{Mg}_2\text{V}_2\text{O}_8$ ($x=0-0.52$) ceramics were synthesized by a conventional solid-state reaction method using high-purity starting powders of analytic-grade $\text{Ba}(\text{OH})_2 \cdot 8\text{H}_2\text{O}$, MgO and V_2O_5 . The raw materials were weighed according to the above formula and then ball-milled for 4 h using zirconia balls and alcohol as the medium on a planetary milling machine. The resulting slurries were then rapidly dried and calcined at 800°C for 4 h in air. The calcined powders were re-milled for 6 h and then mixed together with 5 wt% PVA as a binder. The granulated powders were subsequently pressed into cylinders with dimensions of 10 mm in diameter and 7–8 mm in height. The specimens were first heated at 550°C in air for 4 h to remove the organic binder, and then sintered at $870-960^\circ\text{C}$ for 4 h.

The crystal structure of the fired ceramics was identified via an X-ray diffractometer (XRD, D/Max2500 V, Rigaku, Japan) using $\text{CuK}\alpha$ radiation. The bulk densities of the sintered ceramics were measured by the Archimedes method. The microstructure of the specimens was observed using a field-emission scanning electron microscope (FE-SEM; SU8020, JEOL, Tokyo, Japan) equipped with an energy dispersive spectrometer (EDS). Microwave dielectric properties of the sintered ceramics were measured using a network analyzer (N5230C, Agilent, Palo Alto, CA) and a

temperature chamber (GDW-100, Saiweisi, Changzhou, China). The τ_f values of the samples were measured in the temperature range of $20-80^\circ\text{C}$ and calculated by the following equation:

$$\tau_f = \frac{f_2 - f_1}{f_1(T_2 - T_1)} \quad (1)$$

where f_1 and f_2 represent the resonant frequencies at T_1 and T_2 , respectively.

3 Results and discussion

Figure 1a presents the normalized XRD patterns of $\text{Ba}_{1+x}\text{Mg}_2\text{V}_2\text{O}_8$ ceramics sintered at optimum temperatures for 4 h. Within the range of $-0.02 \leq x \leq 0.02$, all the diffraction peaks matched well with the standard patterns of $\text{BaMg}_2\text{V}_2\text{O}_8$ (JCPDS No. 72-2159) and no secondary phase was detected. This result indicated that a small amount of Ba-deficiency or Ba-excess would not change the crystal structure of the matrix. However, it should be noted that the main diffraction peak of $\text{BaMg}_2\text{V}_2\text{O}_8$ shifted toward lower diffraction angles as x increased from -0.02 to 0.02 , as shown in Fig. 1b, c, indicating that the volume of the matrix lattice increased with increasing x values. To understand this in more details, refinements were carried out by using GSAS software. The refined pattern of the $x=0.01$ sample was selected as a representative, as shown in Fig. 2. And the refined results of $\text{Ba}_{1+x}\text{Mg}_2\text{V}_2\text{O}_8$ ($-0.02 \leq x \leq 0.02$) samples are shown in Table 1. The reliable factors of R_{wp} , R_p and χ^2 values were in the range of 7.5–8.7%, 5.9–6.70%, and 1.33–1.54%, respectively, indicating the refinement result is reliable. The cell volume increased with increasing x from -0.02 to 0.02 , as discussed above. However, at higher x values ($x > 0.02$), a single-phase $\text{BaMg}_2\text{V}_2\text{O}_8$ structure could not be maintained. The peak intensity of the secondary-phase $\text{Ba}_3\text{V}_2\text{O}_8$ increased with the increment of x . $\text{BaMg}_2\text{V}_2\text{O}_8$ adopts a tetragonal structure with I41/acd space group while $\text{Ba}_3\text{V}_2\text{O}_8$ prefers to crystallize in a hexagonal structure with R32/m space group. The big difference in their structures and coordination relations between Ba^{2+} , V^{5+} and O^{2-} in each phase would determine the stable coexistence of these two phases in the sintered bodies [10, 11]. Additionally, Fig. 1b, c show that the main diffraction peaks of $\text{BaMg}_2\text{V}_2\text{O}_8$ and $\text{Ba}_3\text{V}_2\text{O}_8$ shifted toward higher diffraction angles as x increased from 0.04 to 0.52 . Similar peak shift was also found in other vanadates, probably because the evaporation of V_2O_5 and the presence of V^{4+} at higher sintering temperatures would cause a decrease in cell volume [10, 18, 19].

Figure 3 shows the SEM images of $\text{Ba}_{1+x}\text{Mg}_2\text{V}_2\text{O}_8$ ceramics sintered at optimum temperatures for 4 h. All

Fig. 1 **a** XRD patterns of $\text{Ba}_{1+x}\text{Mg}_2\text{V}_2\text{O}_8$ ceramics sintered at optimal temperatures for 4 h, **b** and **c** locally magnified peak profiles indicated in (a)

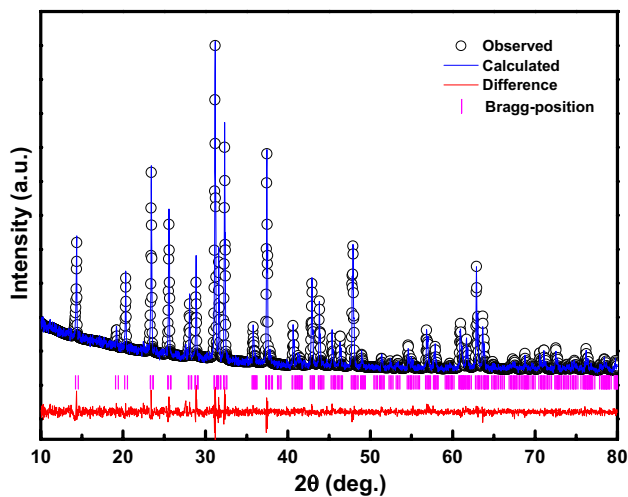
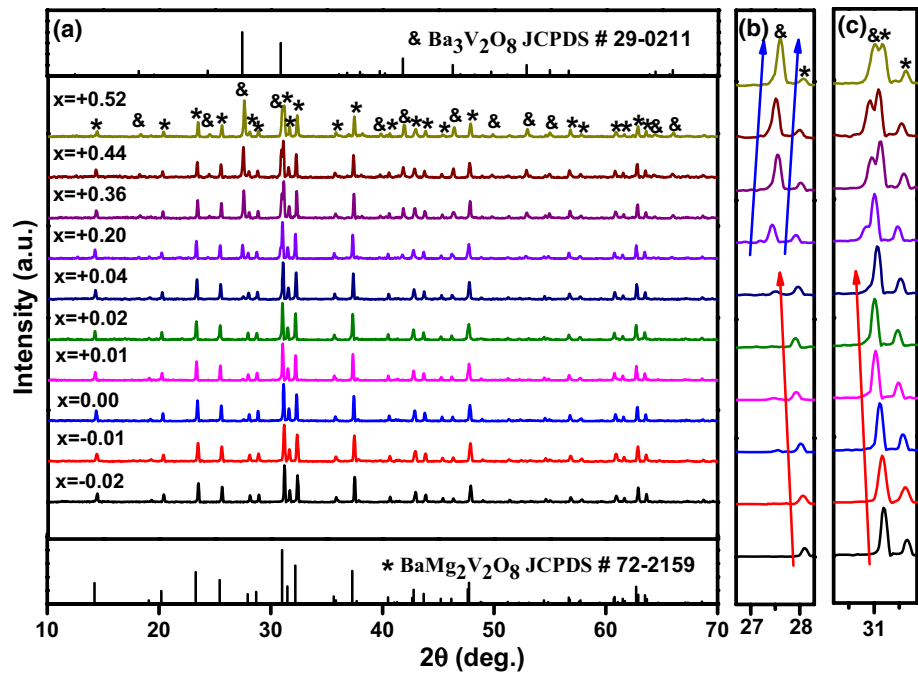


Fig. 2 The Rietveld refinement pattern of the $\text{Ba}_{1.01}\text{Mg}_2\text{V}_2\text{O}_8$ ceramic sintered at 915°C for 4 h

the samples exhibited identifiable grain boundary. Uniform and homogeneous microstructure could be observed in the composition range of $-0.02 \leq x \leq +0.02$, as shown in the Fig. 3a–e. But it should be noted that some small grains began to appear at the grain boundary of the $x = 0.20$ sample and became more with further increasing x values. The variation of grain morphology in $\text{Ba}_{1+x}\text{Mg}_2\text{V}_2\text{O}_8$ ceramics kept a good consistency with the XRD analysis in Fig. 1. That is to say, the $\text{Ba}_{1+x}\text{Mg}_2\text{V}_2\text{O}_8$ ceramics experienced a single-phase solid-solution region and then a diphasic region with increasing x . The EDS analysis was also used to distinguish these two kinds of grains. The EDS results of $x = 0.44$ sample are listed in Table 2. It can be clearly seen that the big grain (marked A) contained Ba, Mg, V and O elements in an approximate molar ratio of Ba:Mg:V:O = 1:2:2:8, which matched with the composition of $\text{BaMg}_2\text{V}_2\text{O}_8$ and the small grain (marked B) mainly contained Ba, V and O elements in an approximate molar ratio of Ba:V:O = 3:2:8, which conformed to the composition of $\text{Ba}_3\text{V}_2\text{O}_8$.

Table 1 Refined unit cell volume, reliability factors and good-of-fit indicator of $\text{Ba}_{1+x}\text{Mg}_2\text{V}_2\text{O}_8$ ceramics ($-0.02 \leq x \leq +0.02$)

	$x = -0.02$	$x = -0.01$	$x = 0$	$x = +0.01$	$x = +0.02$
a=b	12.4077(3)	12.4089(2)	12.4117(2)	12.4124(2)	12.4126(3)
c	8.4562(2)	8.4558(2)	8.4582(2)	8.4590(2)	8.4594(2)
Vol (\AA^3)	1301.84(9)	1302.05(8)	1302.99(7)	1303.27(7)	1303.38(9)
R_{wp} (%)	7.55	8.61	7.87	8.22	7.86
R_{p} (%)	5.92	6.69	6.26	6.43	6.13
χ^2	1.33	1.52	1.47	1.53	1.42

Fig. 3 SEM images of polished and thermally etched $Ba_{1+x}Mg_2V_2O_8$ ceramics sintered at optimal temperatures. **a** $x = -0.02$, 885 °C; **b** $x = -0.01$, 885 °C; **c** $x = 0$, 900 °C; **d** $x = +0.01$, 915 °C; **e** $x = +0.02$, 915 °C; **f** $x = 0.20$, 915 °C; **g** $x = 0.36$, 930 °C; **h** $x = 0.44$, 930 °C and **i** $x = 0.52$, 945 °C

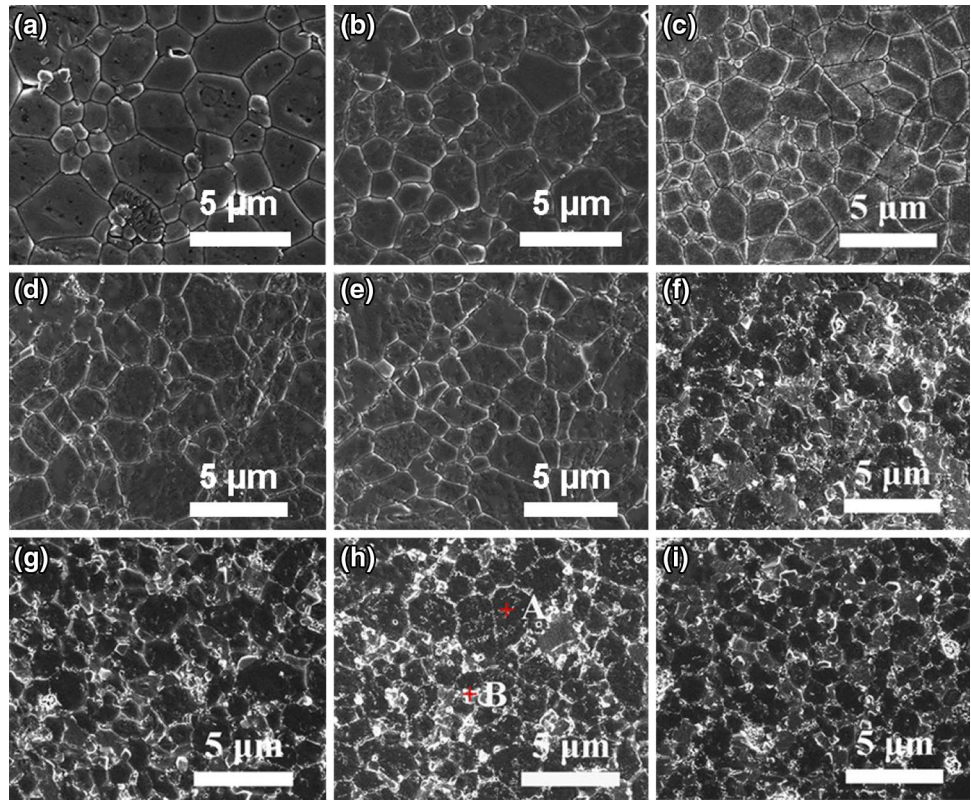


Table 2 EDS results of the $x = 0.44$ sample

Points	Elements (atom %)				Total (%)
	Ba	Mg	V	O	
A	8.05	14.96	16.22	60.77	100.00
B	23.52	1.23	15.88	59.37	100.00

Figure 4 shows the variation of relative density and microwave dielectric properties of $Ba_{1+x}Mg_2V_2O_8$ ($x = -0.02$ to $+0.52$) ceramics as a function of sintering temperature. As shown in Fig. 4a, the relative densities of all studied samples firstly increased to their respective maximum values and then decreased with further increasing sintering temperature. Each composition possessed a high relative density ($>95\%$) at optimum temperatures, keeping a good consistency with the microstructural observation. The variation of ϵ_r and $Q \times f$ values as a function of sintering temperature showed a similar tendency to that of relative density, as can be seen in Fig. 4b, c. The improvement in ϵ_r and $Q \times f$ values with increasing sintering temperature should be mainly related to the enhanced densification, while the evaporation of vanadium and the valance change of V^{5+} at higher sintering temperatures contributed to the subsequent decrease in ϵ_r and $Q \times f$ values [15] in addition to the decline of the sample density. Figure 4d presents the variation of τ_f values as a function of sintering temperature. It can be seen that the τ_f values of each

sample changed little with increasing the sintering temperature, indicating that τ_f was insensitive to sintering temperature. On the other hand, it also can be seen that the ϵ_r values of $Ba_{1+x}Mg_2V_2O_8$ ($x = -0.02$ to $+0.52$) ceramics increased with increasing x values. $Q \times f$ firstly increased up to $x = 0.01$ and thereafter decreased, and τ_f value changed little as x increased from -0.02 to 0.02 but monotonically increased to positive values with a further increase of x . Microwave dielectric properties of $Ba_{1+x}Mg_2V_2O_8$ ceramics within the solid solution range ($-0.02 \leq x \leq 0.02$) and the diphas range ($0.02 < x \leq 0.52$) presented a different variation trend. Thus, a further study was carried out to disclose the relationship between structure and properties.

Figure 5 shows the microwave dielectric properties of $Ba_{1+x}Mg_2V_2O_8$ ceramics in the solid solution range ($-0.02 \leq x \leq +0.02$). The theoretical ϵ_r value can be calculated using the Clausius–Mosotti equation and Shannon additive rule [20] as follows:

$$\alpha_{\text{theo}}(Ba_{1+x}Mg_2V_2O_8) = (1+x)\alpha(Ba^{2+}) + 2\alpha(Mg^{2+}) + 2\alpha(V^{5+}) + 8\alpha(O^{2-}) \quad (2)$$

$$\epsilon_r = \frac{3}{1 - b\alpha_D/V_m} - 2 \quad (3)$$

where α_i ($i = Ba^{2+}, Mg^{2+}, V^{5+}, O^{2-}$) is the polarizability of constituent ions, and b, V_m and ϵ_r represent a constant value

Fig. 4 **a** The relative density, **b** ϵ_r , **c** $Q \times f$, and **d** τ_f values of $\text{Ba}_{1+x}\text{Mg}_2\text{V}_2\text{O}_8$ ($-0.02 \leq x \leq +0.52$) ceramics as a function of sintering temperature

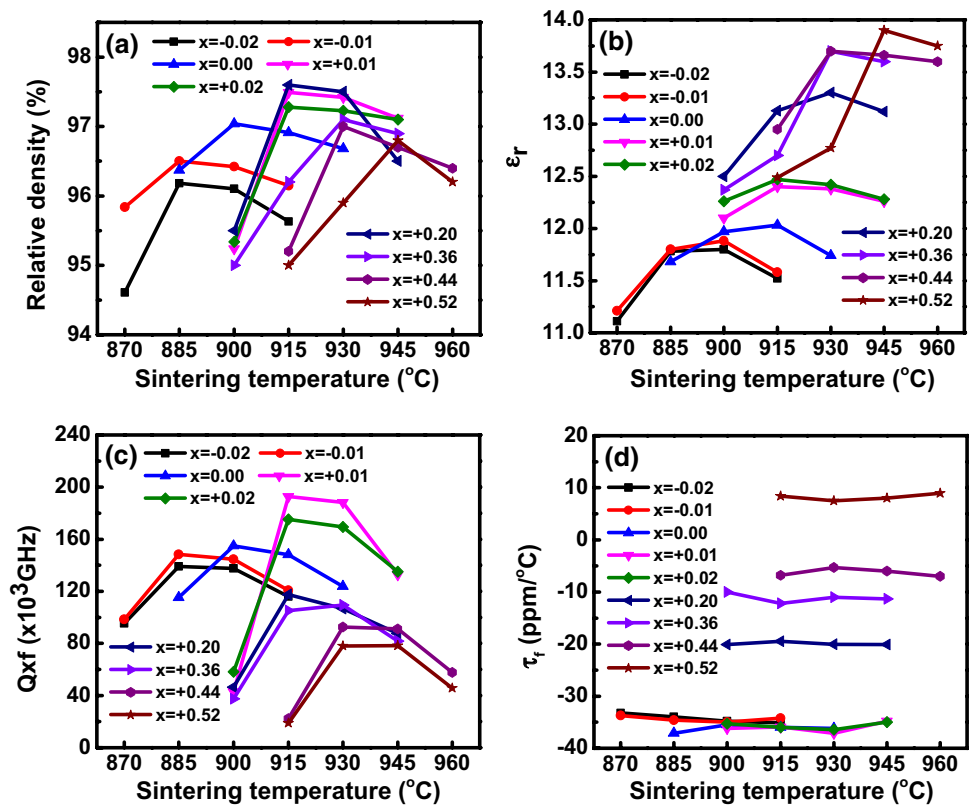
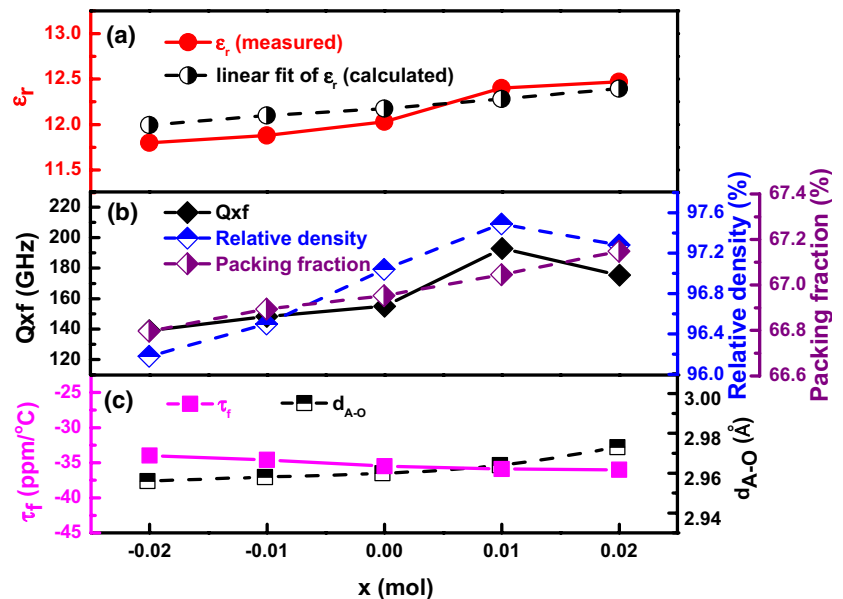


Fig. 5 **(a)** The measured and calculated ϵ_r , **(b)** $Q \times f$ and relative density, and **(c)** τ_f and bond length of $\text{Ba}_{1+x}\text{Mg}_2\text{V}_2\text{O}_8$ ($-0.02 \leq x \leq +0.02$) ceramics as a function of x



($4\pi/3$), molecular volume and dielectric constant, respectively. As can be seen in Fig. 5a, the measured ϵ_r value was close to calculated ϵ_r value and both of them increased with increasing x values. The variation of $Q \times f$ values as a function of x is shown in Fig. 5b. As is well known, the factors that contribute to the dielectric loss can be divided into extrinsic losses and intrinsic losses. The extrinsic losses are

mainly caused by density, secondary phase, grain size and lattice defect while the intrinsic losses are mainly caused by structural characteristics. As shown in Fig. 5b, the packing fraction and relative density both increased with increasing x values, so the $Q \times f$ gradually increased with increasing x values as well. A little decrease in $Q \times f$ at $x=0.02$ could be ascribed to the slight decrease in relative density.

Previous studies revealed the relationship between bond length and τ_f value [21, 22], in which the substitution of smaller Sr^{2+} ions for Ba^{2+} ions decreased A-site average bond length ($d_{\text{A-O}}$) and increased A-site bond valence, thus leading to the increase of τ_f values. As shown in Fig. 5c, τ_f decreased with increasing x values, which corresponded well with the increased A-site average bond length of $\text{Ba}_{1+x}\text{Mg}_2\text{V}_2\text{O}_8$ ceramics. In general, $Q \times f$ was boosted by slightly introducing excessive Ba^{2+} and desirable microwave dielectric properties of $\epsilon_r = 12.4$, $Q \times f = 192,840$ GHz, $\tau_f = -35.3$ ppm/°C were achieved in the $x = 0.01$ sample as sintered at 915 °C for 4 h.

Furthermore, the microwave dielectric properties of the composite ceramic should be related to the volume fraction of each phase in the compounds, which can be described by the following equations [23]:

$$\ln \epsilon_r = V_1 \ln \epsilon_{r1} + V_2 \ln \epsilon_{r2} \quad (4)$$

$$(Q \times f)^{-1} = V_1 (Q \times f)_1^{-1} + V_2 (Q \times f)_2^{-1} \quad (5)$$

$$\tau_f = V_1 \tau_{f1} + V_2 \tau_{f2} \quad (6)$$

where V_1 and V_2 stand for the volume fraction of each phase. The volume fraction of the $\text{Ba}_3\text{V}_2\text{O}_8$ phase was estimated by using the intensity of the strongest peaks for the coexisting phases shown in Fig. 1. The variation of $\ln \epsilon_r$, $(Q \times f)^{-1}$ and τ_f values of $\text{Ba}_{1+x}\text{Mg}_2\text{V}_2\text{O}_8$ ceramics in the diphasic range is shown in Fig. 6. It can be seen that the measured $\ln \epsilon_r$ and τ_f values are close to the calculated values, indicating the mixing rule is applicable. However, the measured $(Q \times f)^{-1}$ values were found to be slightly lower than calculated values. This is probably because the quality factor is more easily influenced by other

factors such as lattice defects, grain size, porosity and so on. Excellent microwave dielectric properties of $\epsilon_r = 13.7$, $Q \times f = 92,580$ GHz, $\tau_f = -5.3$ ppm/°C were obtained in the $x = 0.44$ sample as sintered at 930 °C for 4 h.

4 Conclusions

In present work, the effect of A-site non-stoichiometry on the phase composition, microstructure and microwave dielectric properties of $\text{Ba}_{1+x}\text{Mg}_2\text{V}_2\text{O}_8$ ceramics was investigated. A small amount of Ba-site non-stoichiometry ($-0.02 \leq x \leq 0.02$) did not change the phase structure but significantly boosted the $Q \times f$ value, while a large amount of Ba excess ($0.04 \leq x \leq 0.52$) provoked the $\text{Ba}_3\text{V}_2\text{O}_8$ secondary phase, which acted as a τ_f -modifier in the composite. Good microwave dielectric properties of $\epsilon_r = 12.4$, $Q \times f = 192,840$ GHz, $\tau_f = -35.9$ ppm/°C and $\epsilon_r = 13.7$, $Q \times f = 92,580$ GHz, $\tau_f = -5.3$ ppm/°C were obtained in $\text{Ba}_{1.01}\text{Mg}_2\text{V}_2\text{O}_8$ ceramics sintered at 915 °C for 4 h and in $\text{Ba}_{1.44}\text{Mg}_2\text{V}_2\text{O}_8$ ceramics sintered at 915 °C for 4 h, respectively.

Acknowledgements Financial support from the Anhui Provincial Natural Science Foundation (1508085JGD04) is gratefully acknowledged.

References

1. M.T. Sebastian, H. Jantunen, *Int. Mater. Rev.* **53**, 57 (2008)
2. M. Valant, D. Suvorov, *J. Am. Ceram. Soc.* **83**, 2721 (2000)
3. D. Zhou, H. Wang, L.X. Pang, C.A. Randall, X. Yao, *J. Am. Ceram. Soc.* **92**, 2242 (2009)
4. D. Zhou, L.X. Pang, H. Wang, X. Yao, *J. Eur. Ceram. Soc.* **31**, 2749 (2011)
5. U. Došler, M.M. Kržmanc, B. Jančar, D. Suvorov, *J. Am. Ceram. Soc.* **93**, 3788 (2010)
6. L. Fang, C.X. Su, H.F. Zhou, Z.H. Wei, H. Zhang, *J. Am. Ceram. Soc.* **96**, 688 (2013)
7. Y.P. Liu, Y.N. Wang, Y.M. Li, J.J. Bian, *Ceram. Int.* **42**, 6475 (2016)
8. L. Fang, H.H. Guo, W.S. Fang, Z.H. Wei, C.C. Li, *J. Eur. Ceram. Soc.* **35**, 3765 (2015)
9. Y. Wang, R.Z. Zuo, C. Zhang, J. Zhang, T.W. Zhang, *J. Am. Ceram. Soc.* **98**, 1 (2015)
10. Y. Wang, R.Z. Zuo, *J. Eur. Ceram. Soc.* **36**, 247 (2016)
11. S. Meng, Z. Yue, H. Zhuang et al., *J. Am. Ceram. Soc.* **93**, 359 (2010)
12. G. Yao, C. Pei, H. Ma, et al, *J. Alloys. Compd.* **709**, 234 (2017)
13. C.L. Huang, W.R. Yang, P.C. Yu, *J. Eur. Ceram. Soc.* **34**, 277 (2014)
14. C.F. Xing, J.X. Bi, H.T. Wu, *J. Alloys. Compd.* **719**, 58 (2017)
15. Y. Wang, R.Z. Zuo, *Ceram. Int.* **42**, 10801 (2016)
16. J.J. Bian, G.X. Song, K. Yan, *J. Eur. Ceram. Soc.* **27**, 2817 (2007)
17. K.P. Surendran, M.T. Sebastian, P. Mohanan, R.L. Moreira, A. Dis, *Chem. Mater.* **17**, 142 (2005)
18. C. Zhang, R.Z. Zuo, *J. Alloys. Compd.* **622**, 362 (2015)

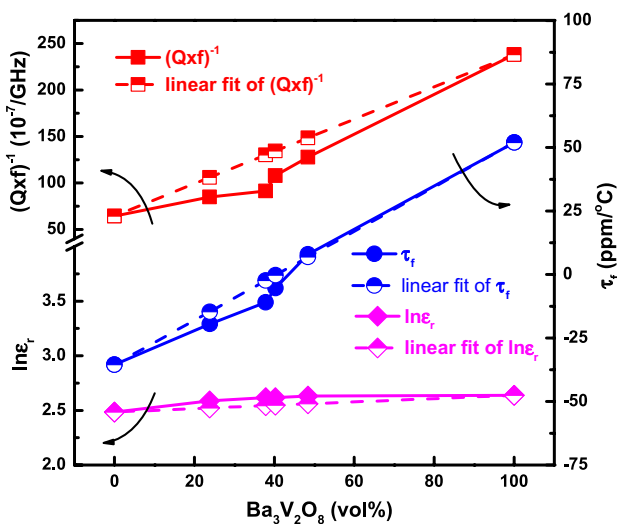


Fig. 6 Microwave dielectric properties of $\text{Ba}_{1+x}\text{Mg}_2\text{V}_2\text{O}_8$ ceramics in the diphasic region as a function of the volume content of $\text{Ba}_3\text{V}_2\text{O}_8$

19. G. Yao, P. Liu, X. Zhao et al., *J. Eur. Ceram. Soc.* **34**, 2983 (2014)
20. Shannon, J. *Appl. Phys.* **73**, 348 (1993)
21. E.S. Kim, B.S. Chun, R. Freer, R.J. Cernik, *J. Eur. Ceram. Soc.* **30**, 1731 (2010)
22. H.S. Park, K.H. Yoon, E.S. Kim, *Mater. Chem. Phys.* **79**, 181 (2003)
23. J. Zhang, R.Z. Zuo, *Mater. Res. Bull.* **83**, 568 (2016)